arXiv:cond-mat/9902111v1 [cond-mat.soft] 9 Feb 1999

Hysteresis and Avalanches in Two Dimensional Foam Rheology Simulations

Yi Jiang[1*], Pieter J. Swart[1], Avadh Saxena[1], Marius Asipauskas[2], James A. Glazier[2]
[1]Theoretical Division, Los Alamos National Laboratory, Los Alamos, NM 87545
[2]Department of Physics, University of Notre Dame, Notre Dame, IN 46556

Foams have unique rheological properties that range from solid-like to fluid-like. We study two-dimensional non-coarsening foams of different disorder under shear in a Monte Carlo simulation, using a driven large-Q Potts model. Simulations of periodic shear on an ordered foam show several different response regimes. At small strain amplitudes, bubbles deform and recover their shapes elastically, and the macroscopic response is that of a linear elastic cellular material. For increasing strain amplitude, the energy-strain curve starts to exhibit hysteresis before any topological rearrangements occur, indicating a macroscopic viscoelastic response. When the applied strain amplitude exceeds a critical value, the yield strain, topological rearrangements (T1 events) occur, the foam starts to flow, and we observe macroscopic irreversibility. We find that the dynamics of topological rearrangements depend sensitively on the structural disorder. Structural disorder decreases the yield strain; sufficiently high disorder changes the macroscopic response of a foam from a viscoelastic solid to a viscoelastic fluid. This wide-ranging dynamical response and the associated history effects of foams result from avalanche-like T1 events. The spatio-temporal statistics of T1 events T1 do not display long-range correlations for ordered foams or at low shear rates, consistent with experimental observations. As the shear rate or structural disorder increases, the topological events become more correlated and their power spectra change from that of white noise toward $1/f$ noise. Intriguingly, the power spectra of the total stored energy also exhibit this $1/f$ trend.

PACS. 83.70.Hq, 82.70.Rr, 02.70.Lq, 46.60.Cn.

I. INTRODUCTION

In addition to their wide-spread industrial importance [1], foams provide significant clues to the rheology of other complex fluids, such as emulsions, colloids and polymer melts, because we can observe their structures directly. The topological structures and the dynamics studied here also occur in other cellular materials, such as biological tissues and polycrystalline alloys. One of the most remarkable and technologically relevant features of foams is the range of mechanical properties that arises from their structure. For sufficiently small stress, foams behave like a solid and are capable of supporting static shear stress. For large stress, foams flow and deform arbitrarily like a fluid. However, we do not yet fully understand the relationship between the macroscopic flow properties of foams and their microscopic details, *e.g.* liquid properties, topological rearrangements of individual bubbles and structural disorder. Constructing a full multiscale theory of foam rheology is challenging. Foams display multiple length scales with many competing time scales, memory effects (*e.g.* the hysteresis discussed in Sec. IV below), and slow aging punctuated by intermittent bursts of activity (*e.g.* the avalanches of T1 events discussed in Sec. V below), all of which severely limit their predictability and control. These problems are intriguing both from an applied and from a fundamental perspective — they provide beautiful concrete examples of multiscale materials, where structure and ordering at the microscale, accompanied by fast and slow time scales, can lead to a highly nonlinear macroscopic response. Here we study the relation between the microscopic topological events and the macroscopic response in two-dimensional non-coarsening foams using a driven extended large-Q Potts model.

In foams, a small volume fraction of fluid forms a continuous network separating gas bubbles [1]. The bubble shapes can vary from spherical to polyhedral, forming a complex geometrical structure insensitive to details of the liquid composition or the average bubble size [2]. Because of the complexity of describing the network of films and vertices in three-dimensional foams, most studies have been two-dimensional. In two-dimensional foams free of stress, all vertices are three-fold and the walls connecting them meet at 120° angles. Minimization of the total bubble wall length dictates that a pair of three-fold vertices is energetically more favorable than a four-fold vertex. Therefore, topology and dynamics are intimately related, with the dominance of three-fold vertices resulting from considerations of structural stability in the presence of surface tension. When shear stress is present, a pair of adjacent bubbles can be squeezed apart by another pair (Fig. 1), leading to a T1 switching event [3]. This local but abrupt topological change results in bubble-complexes rearranging from one metastable configuration to another. The resulting macroscopic dynamics is highly nonlinear and complex, involving large local motions that depend on structures at the bubble

scale. The spatio-temporal statistics of T1 events is fundamental to the plastic yielding of two-dimensional liquid foams.

The nonlinear and collective nature of bubble rearrangement dynamics have made analytical studies difficult, except under rather special assumptions. Computer simulations can therefore provide important insights into the full range of foam behavior. Previous studies in this field can be categorized through their use of constitutive, vertex, center or bubble models.

The constitutive models have evolved from the ideas of Prud'homme [4] and Princen [5]. They modeled foam as a two-dimensional periodic array of hexagonal bubbles where T1 events occur instantaneously and simultaneously for the entire foam. Khan and Armstrong [6] further developed the model to calculate the detailed force balance at the films and vertices, and studied the stress-strain relationships as a function of hexagon orientation, liquid viscosity and liquid fraction. Reinelt and Kraynik [7] extended the same model to study a polydisperse hexagonal foam and derived explicit relations between stress and strain tensors. While analytical calculations exist only for periodic structures or for linear response, foams are naturally disordered with an inherent nonlinear response. Treating the foam as a collection of interacting vertices, vertex models studied the effect of stress on structure and the propagation of defects in foams with zero liquid fraction (*i.e.* dry foam) [3]. Okuzono and Kawasaki [8] studied the effect of finite shear rate by including the force on each vertex, a term which depends on the local motion and is based on the work of Schwartz and Princen [9]. They predicted avalanche-like rearrangements in a slowly driven foam, with a power law distribution of avalanche size *vs.* energy release, characteristic of self-organized criticality. Durian's [10,11] "bubble" model, treating bubbles as disks connected by elastic springs, measured foam's linear rheological properties as a function of polydispersity and liquid fraction. He found similar distributions for the avalanche-like rearrangements with a high frequency cutoff. Weaire *et al.* [12], using a center model based on Voronoi construction from the bubble centers, applied extensional deformation and bulk shear to a two-dimensional foam. They concluded that avalanche-like rearrangements are possible only for wet foams, and that topological rearrangements can induce ordering in a disordered foam. A review by Weaire and Fortes [13] includes some computer models of the mechanical and rheological properties of liquid and solid foams. However, few models have attempted to relate the structural disorder and configuration energy to foam rheology. Only recently, Sollich *et al.* [14], studying mechanisms for storing and dissipating energy, emphasized the role of both structural disorder and metastability in the rheology of soft glassy materials, including foams. Langer and Liu [15], using a bubble model similar to Durian's, found that the randomness of foam packing has a strong effect on the linear shear response of a foam. One of the goals of our study is to quantify the extent of metastability by measuring hysteresis, and relate the macroscopic mechanical response to microscopic bubble structures.

Experiments have measured the macroscopic mechanical properties of three-dimensional foams. But due to the difficulty of direct visualization in three-dimensional foams, no detailed studies of rearrangements exist. Khan *et al.* [16] applied bulk shear to a foam trapped between two parallel plates and measured the stress-strain response, as well as the yield strain as a function of liquid fraction. Princen and Kiss [17], applying shear in a concentric cylinder viscometer (*i.e.* boundary shear), determined the yield stress and shear viscosity of highly concentrated water/oil emulsions. Recently, with the help of diffusing wave spectroscopy (DWS), experiments by Gopal and Durian on three-dimensional shaving creams showed that the rate of rearrangements is proportional to the strain rate, and that the rearrangements are spatially and temporally uncorrelated [2]; Höhler *et al.* [18] found that under periodic boundary shear, foam rearrangements cross from a linear to nonlinear regime; Hébraud *et al.* [19] in a similar experiment on concentrated emulsions, found that some bubbles follow reversible trajectories while others follow irreversible chaotic trajectories. However, none of these experiments has directly observed changes in bubble topology. Dennin and Knobler [20] performed a bulk shear experiment on a monolayer (2D) Langmuir foam and counted the number of bubble side-swapping events. Unfortunately, limited statistics rendered their results difficult to interpret.

In an attempt to reconcile the different predictions of different models and experiments, we use a Monte Carlo model, the extended large-Q Potts model, to study foam rheology. The large-Q Potts model has successfully modeled foam structure, coarsening and drainage [21,22], capturing the physics of foams more realistically than other models. Here we extend the model to include the application of shear to study the mechanical response of two-dimensional foams under stress.

This paper is organized as follows: Sec. II presents our large-Q Potts model; Sec. III contains a description of simulation details; Sec. IV presents results on hysteresis; Sec. V discusses the dynamics and statistics of T1 events; Sec. VI discusses structural disorder and Sec. VII contains the conclusions.

II. MODEL

The great advantage of our extended large-Q Potts model is its simplicity. The model is "realistic" in that the position and diffusion of the walls determine the dynamics, as they do in real foams and concentrated emulsions. Previous models [8,11,12] were based on different special assumptions about the energy dissipation. Since the energy dissipation is poorly understood and also hard to measure in experiments, the exact ranges of validity for these models are not clear. Not surprisingly, these models lead to conflicting predictions, *e.g.* for the distribution of avalanche-like rearrangements (Sec. V). None of these models alone captures the full complexity of real foams.

The extended large-Q Potts model, where bubbles have geometric properties as well as surface properties, is not based on any *a priori* energy dissipation assumption. In addition, it has the advantage of simultaneously incorporating many interactions, including temperature effects, for foams with arbitrary disorder and liquid content [23].

Both the film surface properties and the geometry of bubbles are fundamental to understanding foam flow. The contact angle of walls between vertices indicates whether the structure is at equilibrium, corresponding to minimizing the surface energy. In a real evolving pattern, the equilibrium contact angle occurs only for slow movements during which the vertices remain adiabatically equilibrated. Whenever a topological rearrangement (a T1 event) of the pattern occurs, the contact angles can be far from their equilibrium values. The walls then adjust rapidly, at a relaxation rate depending on the effective foam viscosity, to re-establish equilibrium. The same holds true for the other possible topological change, the disappearance of a bubble, a T2 event [3]. However, disappearance only occurs in foams that do not conserve bubble number and area, which we do not consider in this study. A difficulty in two-dimensional foams is that the effective viscosity depends primarily on the drag between the Plateau borders and the top/bottom surfaces of the container, not the liquid viscosity. Container chemistry, surfactant properties, and foam wetness all change the effective viscosity. Thus even in experiments, the effective viscosity is not equivalent to the liquid viscosity and not possible to derive from liquid viscosity. We define the equilibrium contact angle so that any infinitesimal displacement of the vertex causes a second-order variation of the surface energy, while during a T1 event the energy must vary macroscopically over a small but finite coherence length, typically the rigidity length of a bubble. In our simulations, a bubble under stress can be stretched or compressed up to 60% of its original length, while conserving its area.

In a center model based on the Voronoi construction (see, *e.g.*, [12]), the coherence length of a bubble is comparable to its diameter. Contact angles are given correctly at equilibrium but approach and remain near 90° during a T1 event, since the centers are essentially uninfluenced by topological details such as the difference between a four-fold vertex and a pair of three-fold vertices.

In a vertex model (see, *e.g.*, [8]), the walls connecting the vertices adiabatically follow an out-of-equilibrium, slowly-relaxing vertex. In such a model, the walls are constrained to be straight and vertices typically have arbitrary angles. In essence, the deviation of the vertex angles from the equilibrium value represents the integrated curvature of the bubble walls. Because of their unphysical representation of contact angles, pure vertex models with straight walls cannot handle T1 events correctly.

The extended large-Q Potts model avoids these limitations: walls are free to fluctuate, which is not true in vertex models; and the contact angles during a T1 event are correct, which is not true in center models. A further advantage of our extended large-Q Potts model is that it allows direct measurement of T1 events. The other models cannot directly count T1 events. Instead, they quantify rearrangement events by their associated decreases in energy. We will discuss later this energy decrease is not always directly proportional to the number of T1 events. Our model therefore delivers accurate information about individual T1 events as well as the averaged macroscopic measures such as total bubble wall length, thereby allowing new insights into the connection between microscopic foam structure and macroscopic mechanical response.

Before describing the details of the Potts model, we should first mention its major limitations. Viscosity is one of the basic physical properties of foams, but it is not easily specified *a priori* in the Potts model. Although we can extract the effective viscosity and the viscoelasticity of foams from simulations, we lack a clear quantitative description of the foam viscosity in Potts model simulations and how it relates to the effective and liquid viscosities of a two-dimensional foam. However, our ignorance about simulation viscosity is equivalent to our ignorance about experimental two-dimensional foam viscosity. Quantitative experiments will help to separate the roles of the Plateau borders, fluid viscosity, and topological rearrangements in determining the effective foam viscosity. A second possible limitation is the size effect due to lattice discretization. We show in Sec. III that this problem does not invalidate our simulations. A third drawback is that the Monte Carlo algorithm results in uncertainties in the relative timing of events on the order of a few percent of a Monte Carlo step. While this uncertainty is insignificant for well separated events, it can change the measured interval between frequent events.

The extended large-Q Potts model treats foams as spins on a lattice. Each lattice site $i = (x_i, y_i)$ has an integer "spin" σ_i chosen from $\{1, \ldots, Q\}$. Domains of like spins form bubbles, while links between different spins define the

bubble walls (films). Thus each spin merely acts as a label for a particular bubble. The surface energy resides on the bubble walls only. Since the present study focuses on shear-driven topological rearrangements over many loading cycles, we prohibit foam coarsening by applying an area constraint on individual bubbles. In practical applications, foam deformation and rearrangement under stress is often much faster than gas diffusion through the walls, so neglecting coarsening is reasonable. The Potts Hamiltonian, the total energy of the foam, includes the surface energy and the elastic bulk energy:

$$\mathcal{H} = \sum_{ij} \mathcal{J}_{ij}(1 - \delta_{\sigma_i \sigma_j}) + \Gamma \sum_{n} (a_n - A_n)^2, \tag{1}$$

where $\mathcal{J}_{ij}$ is the coupling strength between neighboring spins σ_i and σ_j, summed over the entire lattice. The first term gives the total surface energy. The second term is the area constraint which prevents coarsening. The strength of the constraint (Γ) is inversely proportional to the gas compressibility; a_n is the area of the nth bubble and A_n its corresponding area under zero applied stress. We can include coarsening by setting Γ to zero.

We extend the Hamiltonian to include shear:

$$\mathcal{H}' = \mathcal{H} + \sum_{i} \gamma(y_i, t) x_i (1 - \delta_{\sigma_i \sigma_j}). \tag{2}$$

The new term corresponds to applying shear strain (a detailed explanation follows below) to the wall between neighboring bubbles σ_i and σ_j, with γ corresponding to the strain field, (x_i, y_i) to the coordinate of spin σ_i and $(1, 0)$ is the direction of the strain.

The system evolves using Monte Carlo dynamics. Our algorithm differs from the standard Metropolis algorithm: we choose a spin at random, but *only* reassign it if it is at a bubble wall and then *only* to one of its unlike neighbors. The probability of accepting the trial reassignment follows the Boltzmann distribution, namely:

$$P \sim \begin{cases} 1 & \Delta\mathcal{H}' < 0 \\ \exp(-\Delta\mathcal{H}'/T) & \Delta\mathcal{H}' \geq 0 \end{cases}, \tag{3}$$

where $\Delta\mathcal{H}'$ is the change in $\mathcal{H}'$ due to a trial spin flip, and T is temperature. Time is measured in units of Monte Carlo steps (MCS), where one MCS consists of as many spin trials as there are lattice sites. This algorithm reproduces the same scaling as classic Monte Carlo methods in simulations of foam coarsening, but significantly reduces the simulation time [24].

The second term in $\mathcal{H}'$ biases the probability of spin reassignment in the direction of increasing x_i (if $\gamma < 0$) or decreasing x_i (if $\gamma > 0$). From dimensional analysis of $\mathcal{H}'$, γ has units of force, but we can interpret it as the strain field for the following reason: In the Potts model a bubble wall segment moves at a speed proportional to the reassignment probability P; in this case,

$$v \propto \sqrt{\gamma} P, \tag{4}$$

where the prefactor follows from dimensional analysis. This shear term effectively enforces a velocity v at the bubble walls, therefore it imposes a strain rate on the foam. The strain $\epsilon(t)$ is then proportional to a time integral of v,

$$\epsilon \propto \int_0^t \sqrt{\gamma(t')} P dt'. \tag{5}$$

If we limit the application of this term to the boundaries of the foam, we impose a boundary shear, equivalent to moving the boundary of the foam with no-slip between bubbles touching the boundary and the boundary, *i.e.*,

$$\gamma = \begin{cases} \gamma_0 G(t) & y_i = y_{\min} \\ -\gamma_0 G(t) & y_i = y_{\max} \\ 0 & otherwise \end{cases}, \tag{6}$$

where γ_0 is the amplitude of the strain field and $G(t)$ is a normalized function of time. On the other hand,

$$\gamma = \beta y_i G(t), \tag{7}$$

with y_i between $y_{\min}$ and $y_{\max}$, corresponds to applying bulk shear with the strain rate varying linearly as a function of position in the foam. The gradient of strain rate is the shear rate, β. The corresponding experiment would be similar to Dennin and Knobler's monolayer Langmuir foam experiment [20]: a monolayer foam (2D) on the surface of

a liquid is sheared in a concentric Couette cell, with no-slip conditions between the bubbles and the container surface. In all our studies we use $G(t) = 1$ for steady shear, and $G(t) = \sin(\omega t)$ for periodic shear. Since for steady shear, the strain is a constant times time, or $\sqrt{\gamma}Pt$, plotting with respect to time is equivalent to plotting with respect to strain.

Note that our driving in the Potts model differs from that in driven spin systems, for which a large body of literature addresses the dynamic phase transition as a function of driving frequency and amplitude [25]. Our driving term acts on the bubble walls (domain boundaries) only, while in driven spin systems *e.g.* the kinetic Ising model, all spins couple to the driving field. The resulting dynamics differ greatly.

III. SIMULATION DETAILS

Experimental observations show that the mechanical responses of a foam, including the yield strain, the elastic moduli, and the topological rearrangements, are sensitive to the liquid volume fraction [26]. In particular, the simulations of both Durian [11] and Weaire *et al.* [12] showed a critical liquid fraction at which a foam undergoes a "melting transition." Although different liquid content and drainage effects can be readily incorporated in the Potts model [22], we focus on the dynamics of topological rearrangements and do not consider liquid fraction dependence of flow behavior, *i.e.* we assume the dry foam limit in this study. Also, we ignore gas diffusion across the walls, assuming that bubble deformation and rearrangement are much faster than coarsening.

The definition of time (Monte Carlo steps or MCS) is not directly related to real time, but we have made choices to ensure that we do not under-resolve events. A shear cycle in the periodic shear case takes about 4000 MCS. In our simulations, a single deformed bubble recovers on a timescale of a few MCS while the relaxation of a cluster of deformed bubbles takes a much longer time, on the order of 10 to 100 MCS. A T1 event by definition takes one MCS (the short life of a four-fold vertex), but the viscous relaxation has to average over at least the four bubbles involved in the T1 event, and thus lasts much longer.

We used periodic boundary conditions in the x direction, to mitigate finite size effects. For ordered foams under boundary shear, we used a 400×100 lattice with each bubble containing 20×20 lattice sites; for ordered foams under bulk shear, we used a 256×256 lattice with 16×16 sites for each bubble. When unstressed, all the bubbles are hexagons, except for those truncated bubbles touching the top and bottom boundaries. In the case of disordered foams, we used a 256×256 lattice with various area distributions. We have also performed simulations using a lattice of size 1024×1024 with 64×64 bubbles and a lattice of size 1024×1024 with 16×16 bubbles. The results did not appear to differ qualitatively. A 16×16 bubble has a side length around 10 lattice sites, so its smallest resolvable tilt angle is approximately $arctan(1/10) \sim 5.7°$. Had lattice effects been a problem, we would have expected a significant difference in the simulations with bubbles of size 64, where the smallest angle is about four times smaller. But increasing the simulation size from 16^2 to 64^2 did not lead to significant changes in the quantities we measured. Thus, we used bubbles of size 16^2 in all the simulations reported in this paper.

Lattice anisotropy can induce artificial energy barriers in lattice simulations. All our runs use a fourth-nearest neighbor interaction on a square lattice, which has a lattice anisotropy of 1.03, very close to the isotropic situation (lattice anisotropy of 1).

Standard quantitative measures of cellular patterns are the topological distributions and correlations, area distributions, and wall lengths — all quantities that in principle can be measured in experiments. Since the areas are constrained, the evolution of the area distribution is not useful. We define the topological distribution $\rho(n)$ as the probability that a bubble has n sides; its m-th moments are $\mu_m \equiv \sum_n \rho(n)(n - \langle n \rangle)^m$. The area distribution $\rho(a)$ and its second moment $\mu_2(a)$ are defined in a similar fashion for the bubble areas. We use a variety of disordered foams with different distributions, as characterized by their $\mu_2(n)$ and $\mu_2(a)$.

In practice, we generate the initial configuration by partitioning the lattice into equal-sized square domains, each containing 16×16 lattice sites. The squares alternate offsets in every other row, so the pattern resembles a brick wall arranged in common bond. We then run the simulation with area constraints, but without strain, at finite temperature for a few Monte Carlo steps, and then decrease the temperature to zero and let the pattern relax. The minimization of total surface energy (and hence the total bubble wall length) results in a hexagonal pattern, the initial configuration for the ordered foam. For disordered initial configurations, we continue to evolve the hexagonal pattern without area constraints at finite temperature so that the bubbles coarsen. We monitor $\mu_2(n)$ of the evolving pattern, and stop the evolution at any desired distribution or degree of structural disorder. Then we relax the patterns at zero temperature with area constraints to guarantee that they have equilibrated, *i.e.* without added external strain or stress the bubbles would not deform or rearrange.

For all our simulations, $\Gamma = 1$ (which is sufficiently large to enforce air incompressibility in bubbles) and $\mathcal{J}_{ij} = 3$ (except when we vary the coupling strength to change the effective viscosity of the foam). Most of the simulations shown in this paper are run at zero temperature except when we study temperature effects on hysteresis, because the

data are less noisy and easier to interpret. A finite but low temperature speeds the simulations, but does not appear to change the results qualitatively.

The number of sides of a bubble is defined by its number of different neighbors. During each simulation, we keep a list of neighbors for each bubble. A change in the neighbor list indicates a topological change which, since bubbles do not disappear, has to be a T1 event.

IV. HYSTERESIS

We can view foam flow as a collective rearrangement of bubbles from one metastable configuration to another. We investigate the configurational metastability by studying hysteresis of the macroscopic response.

Hysteresis is the phenomenon in which the macroscopic state of a system does not reversibly follow changes in an external parameter, resulting in a memory effect. Hysteresis commonly appears in systems with many metastable states due to (but not limited to) interfacial phenomena or domain dynamics. The classic example of the former is that the contact angle between a liquid and a solid surface depends on whether the front is advancing or retreating. The classic example of the latter is ferromagnetic hysteresis, in which the magnetization lags behind the change in applied magnetic field. In cellular materials, including foams, hysteresis can have multiple microscopic origins, including stick-slip interfacial and vertex motion, local symmetry-breaking bubble rearrangement (T1 events), and the nucleation of new and annihilation of old cells. In all of these, noise and disorder play an intrinsic role in selecting among the many possible metastable states arising when the foam is driven away from equilibrium. By focusing on non-coarsening foams, we rule out nucleation and annihilation as sources for hysteresis. Our foam is therefore an ideal testing ground for improving our understanding of hysteresis as it arises from local rearrangements and interfacial dynamics.

In accordance with [8], we define the quantity:

$$\phi \equiv \sum_{i,j} \theta(1 - \delta_{\sigma_i,\sigma_j}), \tag{8}$$

as the total stored elastic energy. Here sites i, j are neighbors, summation is over the whole lattice, and θ is the wall thickness that we choose to be 1 in all our simulations (dry foam limit). Thus ϕ gives essentially the total bubble wall length, which differs by a constant, namely the surface tension, from the total surface energy. In zero temperature simulations, the area constraint is almost always satisfied so that small fluctuations in areas contribute only 10^{-3} of the total energy. Thus we can neglect the elastic bulk energy of the bubbles, and assume that the total foam energy resides on the bubble walls only, *i.e.* all forces concentrate at the bubble walls. We can calculate values of the averaged stress by taking numerical derivatives of the total surface energy with respect to strain [12]. However, the calculation via derivatives is not suitable for foams undergoing many topological changes, since the stored elastic energy changes discontinuously when topological rearrangements occur. The alternative is to calculate stress directly, as given in [27], by the sum of forces acting on the bubble walls, which locally is proportional to the wall length change of a bubble. Because forces on the bubble walls in Potts model foams are not well characterized, we limit our discussions to energy-strain relationships. The more rigorous definition of strain involves the definition of a mesoscopic lengthscale corresponding to a cluster of bubbles, over which the effects of bubble wall orientation and bubble deformation can be averaged. In [8], the average stress tensor, defined as $\sigma = 1/A \sum_{\langle i,j \rangle} |r_{ij}| \hat{r}_{ij} \hat{r}_{ij}$, with A the total area of the foam and r_{ij} the distance between two neighboring vertices, is directly related to ϕ via $\phi = Tr(\sigma)$. Hereafter, we present our ϕ data as $\phi(t)/\phi(0)$ to scale out differences due to initial configurations.

A. Hysteresis in ordered foams

The simplest perturbation which induces topological rearrangements is boundary shear on an ordered foam. In this case we can confine the deformation to the bubbles touching the moving boundaries, and easily locate all the T1 events. As the applied boundary shear increases, the bubbles touching the boundaries distort, giving rise to a stored elastic energy. We show snapshots of the pattern in Fig. 2(a). When a pair of vertices come together to form a four-fold vertex, the numbers of sides changes for the cluster of bubbles involved. Different shades of gray in Fig. 2(a) reflect the topologies of the bubbles. Note that a five-sided (dark grey) and a seven-sided (light grey) bubble always appear in pairs except during the short lifetime of a four-fold vertex (when the number of sides are ambiguous because of the discrete lattice). Once the strain exceeds a critical value, the yield strain, all the bubbles touching the moving boundaries undergo almost simultaneous rearrangements, thereby releasing stress. The stored

elastic energy, ϕ, increases with time when the bubbles deform, then decreases rapidly when the bubbles rearrange. Stress accumulates only in the two boundary layers of bubbles, and never propagates into the interior of the foam. The whole process repeats periodically, due to the periodic bubble structure, as shown in Fig. 2(b), the energy-strain plot (as mentioned at the end of Sec. II, for steady shear, plotting time is equivalent to plotting strain). This result corresponds to the mechanical response obtained in the model of Khan *et al.* with periodic hexagonal bubbles oriented at zero degrees with respect to applied strain [6].

When applying periodic shear $\gamma(t) = \gamma_0 \sin(\omega t)$, we keep the period $2\pi/\omega$ fixed and vary the amplitude, γ_0. Under sinusoidal periodic shear, we observe three types of behavior. When the strain amplitude is small, bubbles deform and recover their shapes elastically when stress is released. No topological rearrangement occurs and the energy-strain plot is linear, corresponding to an elastic response [28]. This result agrees perfectly with the experimental result of DWS in [18]. As the strain amplitude increases, the energy-strain curve begins to exhibit a small butterfly-shaped hysteresis loop before any topological rearrangements occur, indicating a macroscopic viscoelastic response. If we keep increasing the strain amplitude, the hysteresis loop increases in size. When the applied strain amplitude exceeds a critical value, T1 events start occurring, and the foam starts to flow, which leads to a further change in the shape of the hysteresis loop. Even larger strain amplitude introduces more T1 events per period, and adds small loops to the "wings" of the hysteresis loop. Figure 3(a) shows the smooth transition between the three types of hysteresis in the energy-strain curve.

We can adjust the viscosity of the bubble walls by changing the coupling strength $\mathcal{J}_{ij}$. Smaller coupling strength corresponds to lower viscosity. Similar transitions from elastic, to viscoelastic to fluid-like flow behavior occur for progressively lower values of coupling strength, shown in Fig. 3(b). The phase diagram in Fig. 3(c) summarizes 44 different simulations and shows the elastic, viscoelastic and fluid-like behavior (as derived from the hysteretic response) as a function of the coupling strengths $\mathcal{J}_{ij}$ (*i.e.* viscosity) and strain amplitudes γ_0. A striking feature is that the boundaries between these regimes appear to be linear. Figure 3(d) shows the effect of finite temperature on the energy-strain curves. With progressively increasing temperature, noise becomes more dominant and eventually destroys the hysteresis loop. This result implies diminished metastability at finite temperature. However it does not seem to change the trend in mechanical response.

A more conventional experiment is the application of bulk shear [8,11,17,20], with the shear strain varying linearly as a function of the vertical coordinate, from γ_0 at the top of the foam to $-\gamma_0$ at the bottom. In our bulk shear simulations with an ordered foam, the energy-strain relationship has two distinct behaviors depending on the shear rate. At small shear rates, a "sliding plane" develops in the middle of the foam. As shown in Fig. 4(a), non-hexagonal bubbles appear only at the center plane. The energy-strain curve, shown in Fig. 4(b), therefore, resembles that for boundary shear on an ordered foam. The energy curve in Fig. 4(b) also shows that the baseline of energy is larger and that the decrease in amplitude of the energy due to T1s is smaller than in Fig. 2(b), because bulk shear induces a more homogeneous distribution of distortion and thus of stored elastic energy. Again the periodic structure of the bubbles cause the periodicity of the curve, reminiscent of the shear planes observed in metallic glasses in the inhomogeneous flow regime, where stress-induced rearrangement causes plastic deformation [29].

At high shear rates, the ensemble of T1 events no longer localize in space [Fig. 5(a)]. Non-hexagonal bubbles appear throughout the foam. The energy-strain curve, shown in Fig. 5(b), is not periodic but rather smooth; beyond the yield point, the bubbles constantly move without settling into a metastable configuration and correspondingly, the foam displays dynamically induced topological disorder. The transition between these two regimes, localized and nonlocalized T1 events, occurs when the shear rate is in the range $1 \times 10^{-2} < |\beta| < 5 \times 10^{-2}$. This transition can be understood if we look at the relaxation time scale of the foam. Due to surface viscous drag and geometric confinement of other bubbles, the relaxation time for a deformed bubble in a foam is on the order of 10 MCS. For a shear rate $\beta = 5 \times 10^{-2}$, β^{-1} is of the same order as the relaxation time. Thus for shear rates above the natural internal relaxation time scale, the macroscopic response changes from jagged and piece-wise elastic to smooth and viscous response, as observed in fingering experiments in foams [30].

B. Hysteresis in disordered foams

In a disordered foam, bubbles touching the moving foam boundary have different sizes. Boundary strain causes different bubbles to undergo T1 rearrangements at different times. Stress no longer localizes in (sliding) boundary layers, but propagates into the interior [Fig. 6(a)]. The yield strain is much smaller. When the size distribution of the foam is broad, the linear elastic regime disappears, since even a small strain may lead to topological rearrangements of small bubbles. In other words, with increasing degree of disorder, the yield strain decreases to zero and the foam changes from a viscoelastic solid to a viscoelastic fluid. We show an example of such viscoelastic fluid behavior in Fig. 6(b) for a random foam, which shows no energy accumulation, namely, its yield strain is zero. The foam deforms and

yields like a fluid upon application of the smallest strain.

Under a periodic shear, the stored energy increases during an initial transient period but reaches a steady state after a few periods of loading. Energy-strain plots show hysteresis due to topological rearrangements similar to those in ordered foams, but as the degree of disorder increases, the corresponding elastic regime shrinks and eventually disappears.

Rearrangement events in a disordered foam under bulk shear at a low shear rate [snapshots shown in Fig. 7(a)] correspond to those in an ordered foam at a high shear rate. The rearrangements are discrete and avalanche-like, resembling a stick-slip process, or adding sand slowly to a sandpile. However, at sufficiently high shear rate all the avalanches overlap and the deformation and rearrangements are more homogeneous and continuous, as in a simple viscous liquid. Figure 7(b) shows the typical energy-strain curve of a disordered foam under steady bulk shear.

Note that in all our hysteresis plots, the energy-strain curves cross at zero strain, indicating no residual stored energy at zero strain. This crossing is an artifact of our definition of energy, which ignores angular measures of distortion, *i.e.* the total bubble wall length does not distinguish among the directions in which the bubbles tilt. A choice of stress definition which included angular information would show some residual stress at zero strain, but would not affect the results reported here.

V. T1 AVALANCHES

In both experiments [31,32] and our simulations, the contact angles of the vertices remain close to 120° until two vertices meet. The applied strain rate determines the rate at which vertices meet. The resulting four-fold vertex rapidly splits into a vertex pair, recovering 120° contact angles, at a rate determined by the viscosity. This temporal asymmetry in the T1 event contributes to the hysteresis.

In vertex model simulations, sudden releases of energy occur once the applied shear exceeds the yield strain [8]. The event size n, *i.e.* the energy release per event in the dry foam limit, follows a power-law distribution: $\rho(n) \sim n^{-\frac{3}{2}}$. Durian [11] found a similar power-law distribution in his bubble model, with an additional exponential cutoff for large events. Simulations of Weaire *et al.* [12,27], however, suggested that power-law behavior only appeared in the wet foam limit. Experiments, on the other hand, have never found system-wide events or long range correlations among events [2,20]. One of our goals is to reconcile these different predictions.

These differences may result from the use of energy release as proxy for topological changes, rather than enumerating actual events, as well as the assumption of a linear relation between jumps in the stored elastic energy and the number of T1 events, namely, $d\phi/dt = cN$, where N is the number of T1 events and c is a constant. A drastic drop in the total bubble wall length indicates a large number of T1 events. However, in a disordered foam, all T1 events are not equal, since they do not all release the same amount of stored elastic energy. The energy released during a T1 event scales as the bubble perimeter, *i.e.* smaller bubbles release less energy. Hence smaller bubbles undergo more T1 events. Moreover, a T1 event is not strictly local, but deforms its neighborhood over a certain finite range, as demonstrated by T1 manipulations in magnetic fluid foam experiments [33]. Therefore, the number of T1 events is not always directly proportional to the decrease in total bubble wall length. Thus we cannot compare the energy dissipation and T1 events directly. Furthermore, the mechanisms of energy dissipation differ in these models. Kawasaki *et al.* [8] included the dissipation due to the flow of liquid out of the Plateau borders; Durian [11] considered only the viscous drag of the liquid, while Weaire *et al.* [12] modeled an equilibrium calculation involving quasistatic steps in the strain that do not involve any dissipation. In our model, the evolution minimizes the total free energy naturally. To avoid ambiguities, we directly count T1 events in addition to tracking energy.

The avalanche-like nature of rearrangements appears in the sudden decreases of the total elastic energy as a function of time. Figure 4(b) shows the relation between energy and the number of T1 events in an ordered foam under steady bulk shear for a small strain. The stored energy increases almost linearly until the yield strain is reached. The avalanches are well separated. Every cluster of T1 events corresponds to a drastic decrease in the stress, and the periodicity is due to the ordered structure of the foam. At a higher shear rate [Fig. 5(b)], the yield strain remains almost the same, but the avalanches start to overlap and the energy curve becomes smoother. In the sandpile analogy, instead of adding sand grains one at a time and waiting until one avalanche is over before dropping another grain, the grains accumulate at a constant rate and the avalanches, large and small, overlap one another. A sufficiently disordered foam may not have a yield strain [Fig. 6(b)]; T1 events occur at the smallest strain. The foam flows as a fluid without going through an intermediate elastic regime.

To study the correlation between T1 events, we consider the power spectrum of $N(t)$, the number of T1 events at each time step,

$$p_N(f) = \int dt \int d\tau e^{-if\tau} N(t)N(t+\tau), \tag{9}$$

where f is the frequency with unit MCS^{-1}. Figure 8(a) shows typical power spectra of the time series of T1 events in an ordered foam under bulk shear. At a shear rate $\beta = 0.01$, the T1 events show no power law. The peak at $\sim 10^{-3}$ is due to the periodicity of bubble structure in an ordered foam when a "sliding plane" develops. At shear rate $\beta = 0.02$, the spectrum resembles that of white noise. As the shear rate increases to $\beta = 0.05$, the power spectrum develops a power law tail at the low frequency end, with an exponent very close to 1. In a disordered foam, with increasing shear rate, the spectra for the T1 events gradually change from completely uncorrelated white noise to $1/f$ at higher shear rates. By $1/f$, we mean any noise of power spectrum $S(f) \sim f^{-\alpha}$ where $0 < \alpha < 2$ or near 1, *i.e.* intermediate between Brownian noise ($\alpha = 2$) and white noise ($\alpha = 0$).

These power spectra suggest that the experimental results for T1 events as reported in [2,20] correspond to a low shear rate, with no long-range correlation among T1 events. Structural disorder introduces correlations among the events. Power-law avalanches do not occur in ordered hexagonal cells at low shear rate, where rearrangements occur simultaneously. At a high shear rate, when the value of $\dot{\gamma}^{-1}$ is comparable to the duration of rearrangement events, the bubbles move constantly. The foam behaves viscously, since rearrangements are continuously induced before bubbles can relax into metastable configurations which can support stress elastically. At these rates, even an initially ordered structure behaves like a disordered one, as shear destroys its symmetry and periodicity.

In a disordered foam, whenever one T1 event happens, the deformed bubbles release energy by viscous dissipation and also transfer stress to their neighboring bubbles, which in turn are more likely to undergo a T1 switch. Thus, T1 events become more correlated. Shown in Fig. 8(b), the power spectra change from that of white noise toward $1/f$ noise. When the first sufficiently large region to accumulate stress undergoes T1 events, it releases stress and pushes most of the rest of the bubbles over the brink, causing an "infinite avalanche": some bubbles switch neighbors, triggering their neighbors to rearrange (and so on), until a finite fraction of the foam has changed configuration, causing a decrease in the total stored energy, mimicking the cooperative dynamic events in a random field Ising model [34]. We never observe system-wide avalanches as claimed in the vertex model simulations [8], agreeing with Durian's simulations [11] and Dennin *et al.*'s experiments [20]. For even greater disorder, the bubbles essentially rearrange independently, provided spatial correlations for area and topology are weak. Pairs of bubbles switch as the strain exceeds their local yield points. Although more frequent, the avalanches are small, without long correlation lengths. Figure 8(c) shows the power spectra for T1 events for a highly disordered structure with $\mu_2(n) = 1.65$. We observe no power law behavior, even at high shear rates. Thus a highly disordered foam resembles a homogeneous but nonlinear viscous fluid.

Over a range of structural disorder the topological rearrangement events are strongly correlated. The question naturally arises whether the transition between these correlated and uncorrelated regimes is sharp or smooth, and what determines the transition points. We are currently carrying out detailed simulations involving different structural disorder to study this transition.

Previous simulations [11] and experiments [20] measured $\overline{N}$, the average number of T1 events per bubble per unit shear, and concluded that $\overline{N}$ was independent of the shear rate. Our simulation results in three different foams with shear rates covering two orders of magnitude, however, disagree. As shown in Fig. 9, our data indicate that $\overline{N}$ depends sensitively on both the polydispersity of the foam and the shear rate. Only at large shear rates does $\overline{N}$ seem to be independent of the shear rate, which might correspond to the above-mentioned experiments.

The avalanches and $1/f$ power spectra resemble a number of systems with many degrees of freedom and dissipative dynamics which organize into marginally stable states [35]. Simple examples include stick-slip models, driven chains of nonlinear oscillators, and sandpile models. In sandpile models, both the energy dissipation rate (total number of transport events at each time step) and the output current (the number of sand grains leaving the pile) show power-law scaling in their distributions. In particular, if the avalanches do not overlap, then the power spectrum of the output current follows a power law with a finite size cutoff [36]. The $1/f$-type power spectra result from random superposition of individual avalanches [37].

If the analogy with sandpiles holds, we should expect the power spectra of the time derivative $d\phi/dt$, of the stored energy, *i.e.* the energy change at every time step, to be $1/f$-like, and thus the power spectra of ϕ to be f^{-2}. However, in our simulations $d\phi/dt$ does not show $1/f$-type broadband noise. Figures 10 (a-c) show the corresponding power spectra for ϕ from the same simulations as Fig. 8, which are obviously not f^{-2}, *i.e.* the topological rearrangements are not in the same universality class as sandpiles. In particular, Fig. 8(c) shows a complicated trend: the power spectrum changes from a small slope at shear rate $\beta = 0.001$ to $f^{-0.8}$ spanning over 4 decades at $\beta = 0.005$. But as the shear rate increases, the power law disappears. Instead, a flat tail develops at high frequencies due to Gaussian noise. Other different slopes appear over different regimes of different sizes, indicating the existence of multiple time-scales and length-scales. We will further explore the implications of these spectra for ϕ elsewhere [38].

VI. EFFECTS OF STRUCTURAL DISORDER

As structural disorder plays an important role in mechanical response, we study the effect of disorder on the yield strain and the evolution of disorder in foams under shear. We define the yield strain, at which the first T1 avalanches occur, as the displacement at the top boundary of the foam divided by half the height of the foam (since the zero strain is in the middle of the foam) rescaled by the average bubble width.

Figure 11(a) shows the yield strain as a function of shear rate β for different foam disorders. We find that for an ordered foam at low shear rates, when a sliding plane occurs in the middle of the foam, the yield strain is independent of shear rate. We expect this independence because T1 events occur almost simultaneously in the sliding plane, and the bubble size determines the yield strain. At high shear rates, T1 events distribute more homogeneously throughout the foam which lowers the yield strain. The upper limit for the yield strain in an ordered foam is $2/\sqrt{3}$, when all the vertices in a hexagonal bubble array simultaneously become four-fold under shear. The nucleation of topological defects (5-and-7-sided bubble pairs) and their propagation in foams lower the yield strain. But the yield strain does not reach zero even at a very high shear rate of $\beta = 0.05$. An ordered foam remains a solid with finite yield strain. For a disordered foam, the yield strain is lower for higher shear rates; and at the same shear rate, the yield strain decreases drastically to zero as disorder increases — the foam changes from a viscoelastic solid to a viscoelastic fluid.

The most commonly used measure for topological disorder is the second moment of the topological distribution, $\mu_2(n)$. During diffusional foam coarsening, the topological distribution tends to a stationary scaling form and $\mu_2(n)$ assumes a roughly constant value. Experiments on soap foams with up to 10000 bubbles in the initial state [31,32] and early smaller simulations [39] gave a value of $\mu_2(n) = 1.4$ in the scaling regime. Other simulations showed a slightly lower value of $\mu_2 = 1.2$ [40]. Weaire *et al.* [12] reported shear-induced ordering, *i.e.* reduction of $\mu_2(n)$ with shearing. However, in our simulations, foams with initial $\mu_2(n)$ ranging from 0.81 to 2.02 show no shear-induced ordering. Instead, $\mu_2(n)$ increases and never decreases back to its initial unstrained value. Figure 11(b) shows the evolution of $\mu_2(n)$ for a variety of initial topological distributions. The difference between the simulations of Weaire *et al.* [12] and ours is not surprising. Weaire *et al.* applied step strain and observed the resulting equilibrated pattern. In our simulations, bubbles are constantly under shear, *i.e.* the foam is not in equilibrium. The topological disorder, as measured by $\mu_2(n)$, therefore increases as the energy accumulates and decreases as the energy releases, as does the number of topological events, and does not necessarily settle to an equilibrium value.

In an ordered foam at shear rate $\beta = 0.01$ [Fig. 4] with separated T1 avalanches, $\mu_2(n)$ fluctuates in synchrony with the total energy, shown in Fig. 11(c). When the avalanches overlap, $\mu_2(n)$ fluctuates more smoothly, but almost always has a positive correlation with the total stored energy.

Notice that in the energy-strain plots [Fig. 2(b), Fig.4(b)], stored energy slowly increases over long times, because we continuously apply shear and the foam is always out of equilibrium. Bubbles do not fully recover their original shapes. This deformation slowly accumulates at long times. In disordered foams, topological rearrangement may enhance the spatial correlation of bubbles, *i.e.* small bubbles cluster over time, as predicted by Langer and Liu's bubble model [15]. We will report results on spatial correlations for bubble topology n, and area a elsewhere [38].

VII. CONCLUSIONS

We have included a driving term in the large-Q Potts model to apply shear to foams of different disorder. When the driving rate is too fast for the foam to relax, the system falls out of equilibrium. The mechanical response then lags behind the driving shear, resulting in hysteresis. Our model differs from most well studied driven spin models: our spins do not couple to an external field the way Ising spins couple to an oscillating magnetic field, and all action occurs only at the domain boundaries.

Because of the difficulty in characterizing local stress and strain in Potts model foams, we have chosen to use the rescaled total bubble wall length, ϕ, as the order parameter for hysteresis. While the hysteresis loops reflect the nonlinearity and metastability of bubble configurations, it is still an open question whether we can find more appropriate order parameter(s) that will provide more insight into the dynamics of T1 events. Another consequence of this difficulty is the lack of a clear quantitative description of the viscosity in our simulated foams in terms of the model parameters, a difficulty mirrored in the lack of understanding of effective foam viscosity in experiments. As mentioned above, a fundamental problem is the lack of experimental data on the viscosity of two-dimensional foams. We hope that these simulations will motivate new experiments in this direction.

The local cellular patterns characteristic of T1 events in foams are strikingly similar to the low temperature defects and the hexatic-square Voronoi patterns observed in two-dimensional (particle) systems, *e.g.* two-dimensional liquid crystals and colloidal suspensions, where studies have focused on the melting phase transitions [41,42]. This similarity lead us to try the defect description used in melting studies, namely the nearest-neighbor-bond-orientation order

parameter $\sum_n \exp(6i\theta_n)$, where θ_n is the angle between two neighboring bonds. However, we found it insensitive to the orientation change of bubble walls during T1 events and thus not a useful order parameter. How the nucleation and propagation of topological defects in a sheared foam relate to the nucleation and role of topological defects in the two-dimensional melting studies remains an interesting question.

We have demonstrated three different hysteresis regimes in an ordered foam under oscillating shear. At small strain amplitudes, bubbles deform and recover their shapes elastically after stress release. The macroscopic response is that of a linear elastic solid. For larger strain, the energy-strain curve starts to exhibit hysteresis before any topological rearrangements occur, indicating a macroscopic viscoelastic response. Increasing the strain amplitude increases the area of the hysteresis loop. When the applied strain amplitude exceeds a critical value, the yield strain, T1 events occur and the foam starts to flow, and we observe macroscopic irreversibility.

We are currently testing this observation in an experiment similar to [18], applying periodic boundary shear to a homogeneous foam, and measuring the total bubble wall length directly (instead of using diffusion wave spectroscopy) to obtain ϕ. We can directly compare this data with the predicted three distinct behaviors. The viscoelasticity of foams is better characterized using the complex modulus $G(\omega)$ [14], which we plan to use in future investigations.

The comparison between the mechanical responses of ordered and disordered foams provides some insight into the relation between local structure and macroscopic response. An ordered foam has a finite yield strain. Structural disorder decreases the yield strain; sufficiently high disorder changes the macroscopic response of a foam from a viscoelastic solid to a viscoelastic fluid. A random foam with broad topology and area distributions lacks the linear elastic and viscoelastic solid regimes. Any finite stress can lead to topological rearrangements of small bubbles and thus to plastic yielding of the foam. More detailed simulations and experiments are needed to determine the dependence of the yield strain on the area and topological distributions of the foam, and on the shear rates. High shear rates effectively introduce more topological defects into the foam, as manifested in ordered foams driven at high shear rates. Local topological rearrangements (the appearance of non-hexagonal bubbles) occur throughout the foam, resulting in more homogeneous flow behavior, as in disordered foams.

Our simulations show that $\overline{N}$, the average number of T1 events per bubble per unit shear, is sensitive to the area distribution of the foam and the shear rate. Only for a small range of shear rates do foams having similar distributions show similar values of $\overline{N}$, which may explain previous studies [11,20]. Our results emphasize the importance of both structural disorder and configurational metastability to the behavior of soft cellular materials.

In disordered foams, the number of T1 events is not directly proportional to the elastic energy release, because each T1 event is non-local and different T1 events can release different amounts of energy. Therefore, we count T1 events and energy release separately.

Avalanche-like topological rearrangements play a key role in foam rheology. Our simulations show that T1 events do not have finite long-range correlations for ordered structures or at low shear rates, consistent with experimental observations. As the shear rate or structural disorder increases, the topological events become more correlated. Over a range of disorders, the power spectra are $1/f$. As Hwa and Kardar pointed out, $1/f$ noise may arise from a random superposition of avalanches [37]. These $1/f$ spectra suggest that avalanches of different sizes, although they overlap, are independent of each other. Both greater structural disorder and higher shear rate introduce a flat tail at the high frequency end, a signature of Gaussian noise, but do not change the exponent in the power law region.

However, unlike the sandpile model, the power spectra of the total energy, rather than of the energy dissipation, show a similar trend toward $1/f$. One major difference between T1 avalanches and sand avalanches is that each sand grain carries the same energy, while each T1 event can have a different energy. A better analogy may be a "disordered sandpile" model, where the sand grains have different sizes or densities, and avalanches overlap.

Avalanches of T1 events decrease the stored elastic energy, leading to foam flow. How do single T1 events contribute to the global response? Magnetic fluid foam experiments offer a unique opportunity to locally drive a vertex and force a single T1 event (or a T1 avalanche) by a well-controlled local magnetic field. We are investigating the effects of single T1 events using magnetic fluid foam experiments and the corresponding Potts model simulations [43].

ACKNOWLEDGMENT

We would like to thank F. Graner, M. Sano, S. Boettcher and I. Mitkov for fruitful discussions. This work was supported in part by NSF DMR-92-57001-006, ACS/PRF and NSF INT 96-03035-0C, and in part by the US Department of Energy.

---

* Contact author: CNLS, MS B258, Los Alamos National Laboratory, Los Alamos, NM 87544. Email: jiang@lanl.gov

[1] A. M. Kraynik, Ann. Rev. Fluid Mech. **20**, 325 (1988).
[2] A. D. Gopal and D. J. Durian, Phys. Rev. Lett. **75**, 2610 (1995).
[3] D. Weaire and N. Rivier, Contemp. Phys. **25**, 55 (1984).
[4] R. K. Prud'homme, Ann. Meet. Soc. Rheol., Lexington, KY (1981).
[5] H. M. Princen, J. Colloid Interface Sci. **91**, 160 (1983).
[6] S. A. Khan and R. C. Armstrong, J. Non-Newtonian Fluid Mech. **22**, 1 (1986); S. A. Khan and R. C. Armstrong, *ibid* **25**, 61 (1987).
[7] D. A. Reinelt and A. M. Kraynik, J. Fluid Mech. **215**, 431 (1990).
[8] T. Okuzono and K. Kawasaki, Phys. Rev. E **51**, 1246 (1995).
[9] L. W. Schwartz and H. M. Princen, J. Colloid Interface Sci. **118**, 201 (1987).
[10] D. J. Durian, Phys. Rev. Lett.**75**,4780 (1995).
[11] D. J. Durian, Phys. Rev. E. **55**, 1739 (1997).
[12] D. Weaire, F. Bolton, T. Herdtle, and H. Aref, Phil. Mag. Lett. **66**, 293 (1992).
[13] D. Weaire and M. A. Fortes, Adv. Phys. **43**, 685 (1994).
[14] P. Sollich, F. Lequeux, P. Hébraud, and M. E. Cates, Phys. Rev. Lett. **78**, 2020 (1997).
[15] S. A. Langer and A. J. Liu, J. Phys. Chem. B **101** 8667 (1997).
[16] S. A. Khan, C. A. Schnepper, and R. C. Armstrong, J. Rheol. **31**, 69 (1988).
[17] H. M. Princen and A. D. Kiss, J. Colloid Interface Sci. **112**, 427 (1986).
[18] R. Höhler, S. Cohen-Addad, and H. Hoballah, Phys. Rev. Lett. **79**, 1154 (1997).
[19] P. Hébraud, F. Lequeux, J. P. Munch, and D. J. Pine, Phys. Rev. Lett. **78** 4657 (1997).
[20] M. Dennin and C. M . Knobler, Phys. Rev. Lett. **78**, 2485 (1997).
[21] See, *e.g.*, J. A. Glazier, M. P. Anderson and G. S. Grest, Phil. Mag. B **62**, 615 (1990); J. A. Glazier, Phys. Rev. Lett. **70**, 2170 (1993).
[22] Y. Jiang and J. A. Glazier, Phil. Mag. Lett. **74**, 119 (1996); Y. Jiang and J. A. Glazier, MRS Symp. Proc. **463**, 307 (1997).
[23] Liquid can be included as a special "phase" of spin; the coupling strengths now depend on the gas and liquid phases, see [22].
[24] B. Radhakrishnan and T. Zacharia, Metal. and Mat. Trans. **26A**, 167 (1995).
[25] See, *e.g.* M. Acharyya and B. K. Chakrabarti, Phys. Rev. B **52**, 6550 (1995); and references therein.
[26] D. Weaire, N. Pittet, S. Hutzler, and D. Pardal, Phys. Rev. Lett., **71**, 2670 (1993).
[27] S. Hutzler, D. Weaire, and H. Bolton, Phil. Mag. B **71**, 277 (1995).
[28] In a linear elastic cellular solid, the shearing displacement of boundary bubble walls is *linearly* proportional to the total boundary wall length. See L. J. Gibson and M. F. Ashby, Cellular Solids: Structure and Properties, Oxford; New York : Pergamon Press, 1988.
[29] F. Spaepen, Acta Metall. **25**, 407 (1997).
[30] S. S. Park and D. J. Durian, Phys. Rev. Lett. **72**, 3347 (1994).
[31] J. A. Glazier, Ph.D. thesis, University of Chicago, 1989, (unpublished).
[32] J. Stavans and J. A. Glazier, Phys. Rev. Lett. **62**, 1318 (1989).
[33] F. Elias, C. Flament, J.-C. Bacri, and F. Graner, in Foams and Emulsions, eds. J.-F. Sadoc and N. Rivier, (Kluwer, Amsterdam, 1998).
[34] J. P. Sethna, K. Dahmen, S. Kartha, J. Krumhansl, B. W. Roberts, and J. D. Shore, Phys. Rev. Lett. **70**, 3347 (1993).
[35] P. Bak, C. Tang, and K. Wiesenfeld, Phys. Rev. Lett. **59**, 381 (1987); Phys. Rev. A **38**, 364 (1988).
[36] H. J. Jensen, K. Christensen, and H. C. Fogedby, Phys. Rev. B **40**, 7425 (1989); K. Christensen, H. C. Fogedby, and H.J. Jensen, J. Stat. Phys. **63**, 653 (1991).
[37] T. Hwa and M. Kardar, Phys. Rev. A **45**, 7002 (1992).
[38] Y. Jiang and J. A. Glazier, in preparation.
[39] D. Weaire and H. Lei, Phil. Mag. Lett. **63**, 1318 (1990).
[40] T. Herdtle and H. Aref, J. Fluid Mech., **241**, 233 (1992).
[41] K. J. Strandburg, Rev. Mod. Phys. **60**, 161 (1988).

[42] D. Deng, A. S. Argon, and S. Yip, Philos. Trans. Royal Soc. London A, **329**, 549 (1989).
[43] F. Elias, C. Flament, F. Graner, J. A. Glazier and Y. Jiang, to appear in Phil. Mag. B (1999).

FIGURE CAPTIONS

Figure 1. Schematic diagram of a T1 event, where bubbles a, b, c and d swap neighbors. Notice that as the edge between the pair of vertices shrinks, the contact angles not in contact with this edge remain 120°.

Figure 2. An ordered foam under boundary shear: (a) Snapshots; different shades of grey encode bubble topologies (lattice size 256×256). (b) Energy-strain curve and the number of T1s presented in 50 MCS bins.

Figure 3. Energy-strain curves for ordered foam under periodic boundary shear: (a) Numbers above the figures are γ_0. Progressively increasing shear amplitude at $\mathcal{J}_{ij} = 3$ leads to a transition between three types of hysteresis: $\gamma_0 = 1.0$ corresponds to an elastic response, $\gamma_0 = 3.5$ shows viscoelastic response (before any T1 event occurs), $\gamma_0 = 7.0$ is a typical response when only one T1 event occurs during one cycle of strain loading. The intermediate steps show that the transition between these three types is smooth. (b) Numbers above the figures are $\mathcal{J}_{ij}$. Progressively decreasing liquid viscosity (increasing $\mathcal{J}_{ij}$ at $\gamma_0 = 7$) shows a similar transition between elastic ($\mathcal{J}_{ij} = 10$) and viscoelastic ($\mathcal{J}_{ij} = 5$) regimes, and flow due to T1 events ($\mathcal{J}_{ij} = 3$ for one T1 event and $\mathcal{J}_{ij} = 1$ for three T1 events during one strain cycle. (c) Phase diagram of hysteresis in the parameter space γ_0 *vs.* $\mathcal{J}_{ij}$; (d) Effect of progressively increasing temperature T ($\mathcal{J}_{ij} = 3$, $\gamma_0 = 4$). All data shown here are averaged over 10 periods.

Figure 4. An ordered foam under bulk shear with shear rate $\beta = 0.01$: (a) Snapshots; shades of grey encode bubble topologies as in Fig. 2. (b) Energy-strain curve and the number of T1s. The magnified view in the box shows the correlation between stress releases and overlapping avalanches of T1 events.

Figure 5. An ordered foam under bulk shear with shear rate $\beta = 0.05$: (a) Snapshots; (b) Energy-strain curve and the number of T1s. The magnified view in the box shows the correlation between stress releases and overlapping avalanches of T1 events.

Figure 6. A disordered foam under boundary shear: (a) Snapshots; shades of grey encode bubble topologies (lattice size 256×256). (b) Energy-strain curve and number of T1 events presented in 100 MCS bins.

Figure 7. A disordered foam under bulk shear at shear rate $\beta = 0.01$: (a) Snapshots; shades of grey encode bubble topologies (lattice size 256×256): (b) Energy-strain curve and number of T1 events.

Figure 8. Power spectra of the number of T1 events: (a) An ordered foam for three shear rates $\beta = 0.01$, 0.02 and 0.05 respectively; (b) A disordered foam $[\mu_2(n) = 0.81, \mu_2(a) = 7.25]$ for five shear rates from 0.001 to 0.05; (c) A very disordered foam $[\mu_2(n) = 1.65, \mu_2(a) = 21.33]$ for three shear rates.

Figure 9. Number of T1 events per unit shear per bubble as a function of shear rate for four foams: squares correspond to a foam of 180 bubbles, with $\mu_2(n) = 1.65$, $\mu_2(a) = 21.33$; stars correspond to a foam of 246 bubbles with $\mu_2(n) = 1.72$, $\mu_2(a) = 15.1$; triangles correspond to a foam of 377 bubbles, with $\mu_2(n) = 1.07$, $\mu_2(a) = 2.50$; and circles correspond to a foam of 380 bubbles, with $\mu_2(n) = 0.95$, $\mu_2(a) = 2.35$. The inset shows on a log-log scale that $\overline{N}$ varies by several orders of magnitude.

Figure 10. Power spectra of the energy: (a) An ordered foam for three shear rates. (b) A disordered foam $[\mu_2(n) = 0.81, \mu_2(a) = 7.25]$ for five shear rates. (c) A very disordered foam $[\mu_2(N) = 1.65, \mu_2(a) = 21.33]$ for five shear rates.

Figure 11. (a) Yield strain as a function of shear rate. (b) Evolution of $\mu_2(n)$ under constant bulk shear, legend denotes the initial $\mu_2(n)$. (c) Evolution of $\mu_2(n)$ under steady bulk shear for an ordered foam, showing the correlation between the stress decreases and $\mu_2(n)$;

This figure "fig1.gif" is available in "gif" format from:

http://arXiv.org/ps/cond-mat/9902111v1

This figure "fig2a.gif" is available in "gif" format from:

http://arXiv.org/ps/cond-mat/9902111v1

This figure "fig2b.gif" is available in "gif" format from:

http://arXiv.org/ps/cond-mat/9902111v1

This figure "fig3a.gif" is available in "gif" format from:

http://arXiv.org/ps/cond-mat/9902111v1

This figure "fig3b.gif" is available in "gif" format from:

http://arXiv.org/ps/cond-mat/9902111v1

This figure "fig3c.gif" is available in "gif" format from:

http://arXiv.org/ps/cond-mat/9902111v1

This figure "fig3d.gif" is available in "gif" format from:

http://arXiv.org/ps/cond-mat/9902111v1

This figure "fig4a.gif" is available in "gif" format from:

http://arXiv.org/ps/cond-mat/9902111v1

This figure "fig4b.gif" is available in "gif" format from:

http://arXiv.org/ps/cond-mat/9902111v1

This figure "fig5a.gif" is available in "gif" format from:

http://arXiv.org/ps/cond-mat/9902111v1

This figure "fig5b.gif" is available in "gif" format from:

http://arXiv.org/ps/cond-mat/9902111v1

This figure "fig6a.gif" is available in "gif" format from:

http://arXiv.org/ps/cond-mat/9902111v1

This figure "fig6b.gif" is available in "gif" format from:

http://arXiv.org/ps/cond-mat/9902111v1

This figure "fig7a.gif" is available in "gif" format from:

http://arXiv.org/ps/cond-mat/9902111v1

This figure "fig7b.gif" is available in "gif" format from:

http://arXiv.org/ps/cond-mat/9902111v1

This figure "fig8a.gif" is available in "gif" format from:

http://arXiv.org/ps/cond-mat/9902111v1

This figure "fig8b.gif" is available in "gif" format from:

http://arXiv.org/ps/cond-mat/9902111v1

This figure "fig8c.gif" is available in "gif" format from:

http://arXiv.org/ps/cond-mat/9902111v1

This figure "fig9.gif" is available in "gif" format from:

http://arXiv.org/ps/cond-mat/9902111v1

This figure "fig10a.gif" is available in "gif" format from:
http://arXiv.org/ps/cond-mat/9902111v1

This figure "fig10b.gif" is available in "gif" format from:
http://arXiv.org/ps/cond-mat/9902111v1

This figure "fig10c.gif" is available in "gif" format from:
http://arXiv.org/ps/cond-mat/9902111v1

This figure "fig11a.gif" is available in "gif" format from:

http://arXiv.org/ps/cond-mat/9902111v1

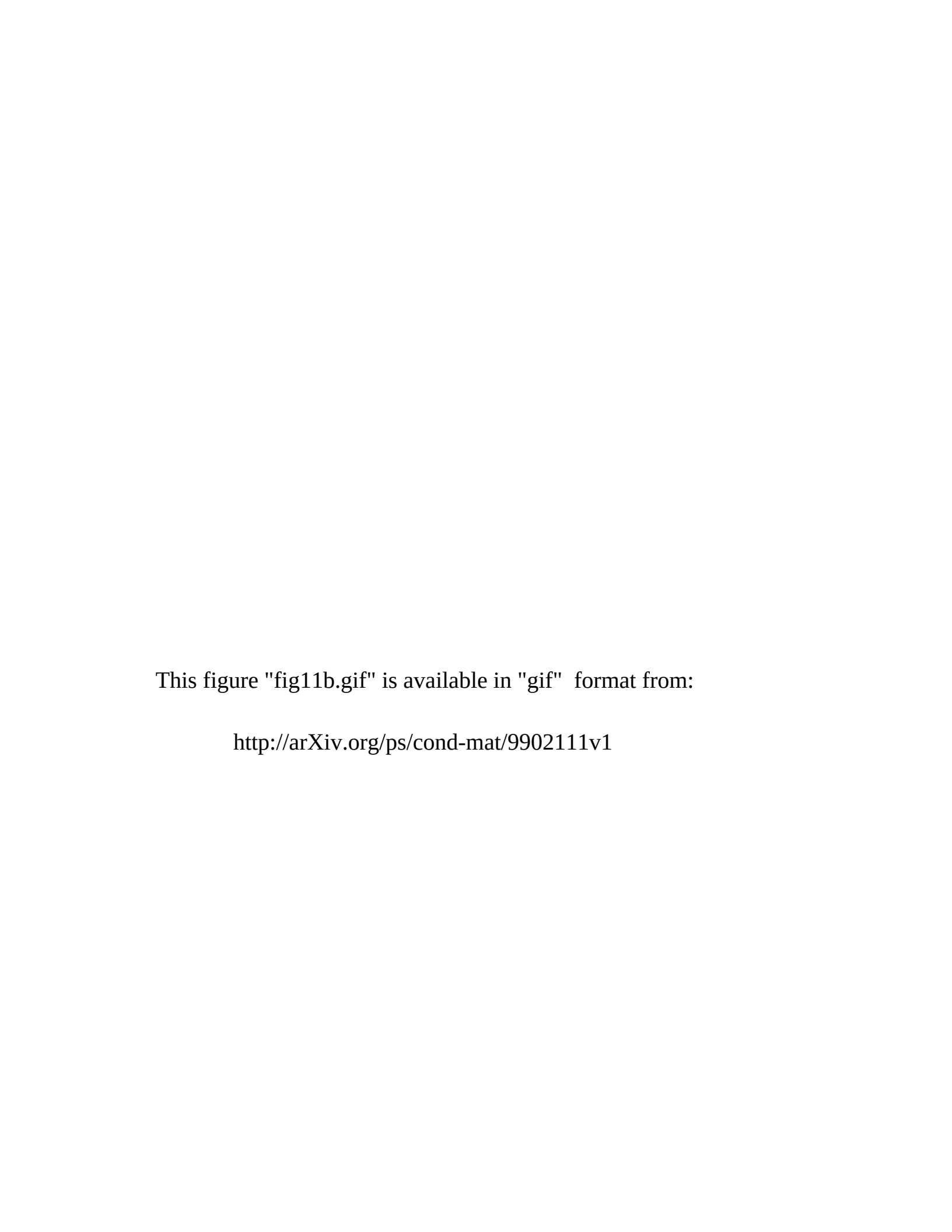
This figure "fig11b.gif" is available in "gif" format from:
http://arXiv.org/ps/cond-mat/9902111v1

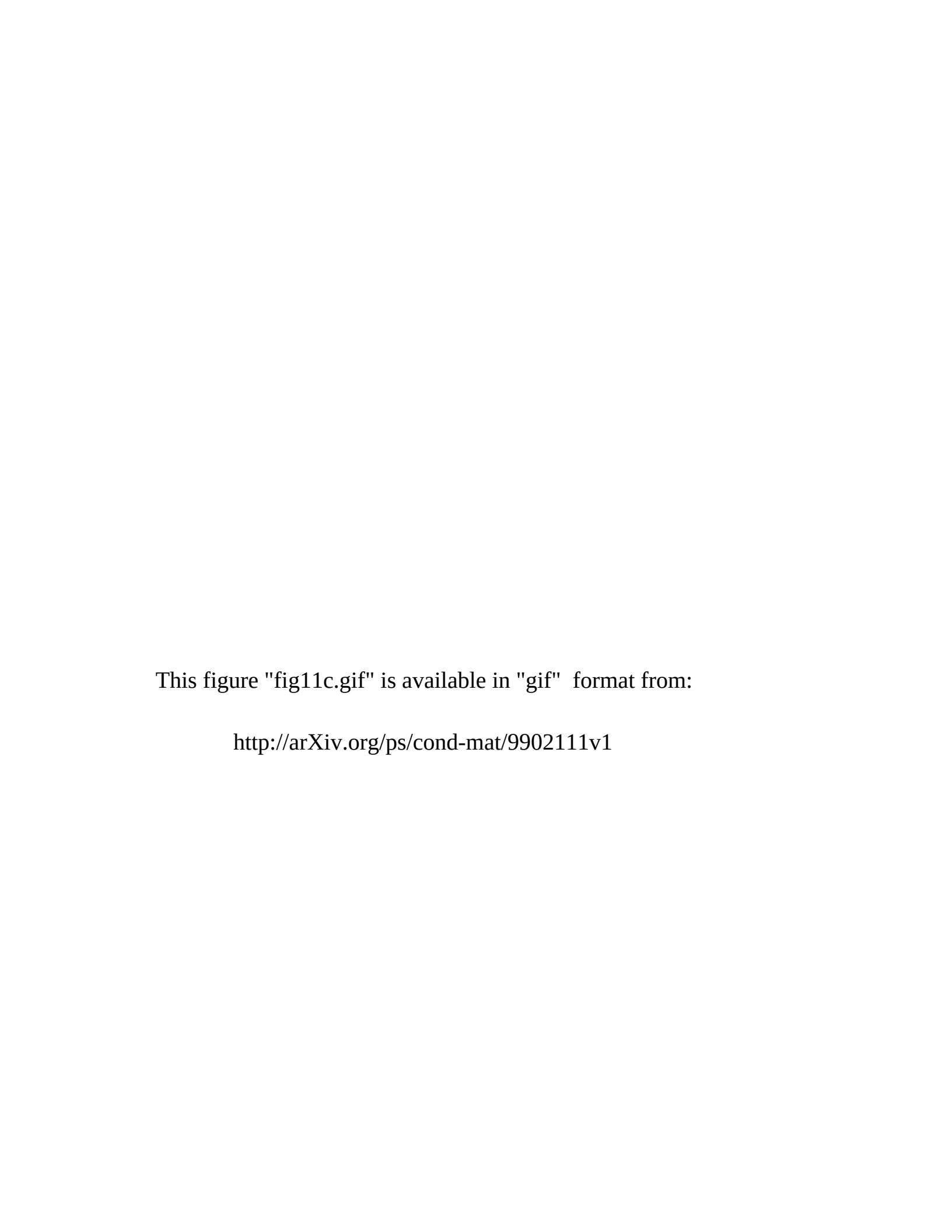
This figure "fig11c.gif" is available in "gif" format from:
http://arXiv.org/ps/cond-mat/9902111v1